ELSEVIER

Journal of Alloys and Compounds 354 (2003) 115–119

Journal of ALLOYS AND COMPOUNDS

www.elsevier.com/locate/jallcom

Synthesis and characterization of the wide band-gap compound $Pr_2Te_4O_{11}$

Ismail Ijjaali, Christine Flaschenriem, James A. Ibers*

Department of Chemistry, Northwestern University, 2145 Sheridan Road, Evanston, IL 60208-3113, USA

Received 20 August 2002; accepted 13 January 2003

Abstract

Single crystals of $Pr_2Te_4O_{11}$ have been grown through the reaction of Pr_6O_{11} and TeO_2 in a CsCl flux at 1123 K. This compound, which is isostructural with $Nd_2Te_4O_{11}$ and $Ho_2Te_4O_{11}$, crystallizes in space group $C2/c$ of the monoclinic system with four formula units in a cell of dimensions at 153 K of $a=12.6880(6)$ Å, $b=5.2361(3)$ Å, $c=16.2920(8)$ Å, $\beta=106.052(1)°$, and $V=1040.17(9)$ Å^3. The three dimensional structure is made from the interconnection between $^2_\infty[Pr_2O_{10}^{14-}]$ and $^2_\infty[Te_4O_{11}^{6-}]$ networks. $Pr_2Te_4O_{11}$ is a Curie–Weiss paramagnetic with an effective magnetic moment of 3.59(2) μ_B. Optical diffuse reflectance spectroscopy shows typical 4f–4f optical transitions for Pr(III), in addition to a wide band gap of 3.65 eV.

Keywords: Synthesis; Crystal structure; Solid-state compound; Praseodymium; Tellurite

1. Introduction

Rare-earth oxides of the general formula $Ln_2Te_4O_{11}$ (Ln=La–Lu) afford the systematic study of the spectroscopic properties of the trivalent lanthanide ions [1–6]. Moreover, oxides containing a metal center with a lone pair of electrons, including the present case of Te(IV), are important luminescence activators [7,8]. Structural studies on the $Ln_2Te_4O_{11}$ (Ln=La–Lu) compounds are confined to X-ray powder diffraction measurements except for single-crystal studies of $Nd_2Te_4O_{11}$ [9] and $Ho_2Te_4O_{11}$ [10]. Here we describe the synthesis and structure of $Pr_2Te_4O_{11}$, together with its magnetic and optical properties.

2. Experimental

2.1. Synthesis

Single crystals of $Pr_2Te_4O_{11}$ were prepared from the reaction of Pr_6O_{11} (Aldrich, 99.999%) and TeO_2 in a molar ratio of 1:4. TeO_2 was synthesized by dissolving Te metal in aqua regia at 353 K, followed by the slow addition of NH_4OH. The resultant precipitate of TeO_2 was filtered and washed with deionized water. Its purity was established by means of a powder X-ray diffraction pattern. A CsCl (Strem, 99.9%) flux in approximately five times molar excess was used to promote single-crystal growth. The starting materials were mixed together and placed in a fused-silica tube, which was then evacuated to $\sim 10^{-5}$ Torr and sealed. The tube was heated to 1123 K at 10 K/h, kept at 1123 K for 6 days, cooled at 2.5 K/h to 873 K, and then the furnace was turned off. The reaction mixture was washed free of chloride salts with water and then dried with acetone. Pale green plate-like crystals of $Pr_2Te_4O_{11}$ suitable for X-ray structure analysis were produced in very high yield. The compound is stable in air and water. Semiquantitative analyses performed with a Hitachi 3500N SEM confirmed the presence of Pr and Te in the approximate ratio of 1:2.75, in reasonable agreement with that of 1:2 from the X-ray structure determination. Oxygen was detected but could not be quantified.

2.2. Crystallography

A single crystal of $Pr_2Te_4O_{11}$ was mounted on the end of a glass fiber and placed in the cold stream of a Bruker SMART-1000 CCD diffractometer [11]. The crystal was kept at 153 K throughout the data collection. X-ray diffraction data were collected with the use of monochromatized Mo Kα radiation ($\lambda=0.71073$ Å). The dif-

*Corresponding author. Tel.: +1-847-491-5449; fax: +1-847-491-2976.

E-mail address: ibers@chem.northwestern.edu (J.A. Ibers).

0925-8388/03/$ – see front matter
doi:10.1016/S0925-8388(03)00190-7

Table 1
Crystal data and structure refinement for $Pr_2Te_4O_{11}$

Formula weight	968.22
Space group	$C2/c$
a (Å)	12.6880(6)
b (Å)	5.2361(3)
c (Å)	16.2920(8)
β (°)	106.052(1)
Volume (Å^3)	1040.17(9)
Z	4
T (K)	153(2)
λ (Mo Kα) (Å)	0.71073
ρ_c (g/cm^3)	6.183
Crystal dimensions (mm)	0.12×0.12×0.08
μ (cm^{-1})	203.0
Transmission factors	0.107–0.259
Total reflections/unique reflections	5725/1268
$R(F)$[a] ($F_o^2 > 2\sigma(F_o^2)$)	0.0185
$R_w(F_o^2)$[b] (all data)	0.0507

[a] $R(F) = \Sigma||F_o| - |F_c||/\Sigma|F_o|$.
[b] $R_w(F_o^2) = [\Sigma\, w(F_o^2 - F_c^2)^2/\Sigma\, wF_o^4]^{1/2}$, $w^{-1} = \sigma^2(F_o^2) + (0.02 \times F_o^2)^2$ for $F_o^2 > 0$; $w^{-1} = \sigma^2(F_o^2)$ for $F_o^2 \leq 0$.

fracted intensities generated by a scan of 0.3° in ω were recorded on sets of 606 frames at ϕ angles of 0°, 90°, 180°, and 270°. The exposure time was 15 s/frame. Final unit cell parameters were obtained by a global refinement of the positions of 4597 reflections with the use of the processing program SAINT Plus [11]. A face-indexed absorption correction was applied with the use of the program XPREP [12] and the program SADABS [11], which relies on redundancy in the data, was then used to apply some semi-empirical corrections for frame variations. The structure was solved with the use of the direct-methods program SHELXS and refined by full-matrix least-squares techniques with the use of the program SHELXL of the SHELXTL suite of programs [12]. The program STRUCTURE TIDY [13] was used to standardize the positional parameters. The final refinement included anisotropic displacement parameters. Additional crystallographic parameters are given in Table 1. Positional parameters and equivalent isotropic displacement parameters are given in Table 2.

Table 2
Atomic coordinates and equivalent isotropic displacement parameters for $Pr_2Te_4O_{11}$

Atom	x	y	z	U_{eq}[a]
Pr	0.118934(16)	0.24417(3)	0.537623(13)	0.00484(9)
Te(1)	0.119832(18)	0.22957(6)	0.203026(16)	0.00552(9)
Te(2)	0.370479(18)	0.27757(7)	0.128620(14)	0.00439(9)
O(1)	0.02662(15)	0.0948(4)	0.10135(12)	0.0093(4)
O(2)	0.20675(15)	0.0394(3)	0.44219(12)	0.0096(4)
O(3)	0.25055(15)	0.0664(4)	0.12967(12)	0.0102(4)
O(4)	0.35236(16)	0.0547(3)	0.32733(12)	0.0104(4)
O(5)	0.42763(15)	0.1205(3)	0.04715(12)	0.0102(4)
O(6)	0	0.3542(5)	1/4	0.0114(6)

[a] U_{eq} is defined as one third of the trace of the orthogonalized U_{ij} tensor.

2.3. Magnetic susceptibility measurements

A 100.7-mg sample of $Pr_2Te_4O_{11}$ single crystals was ground to a fine powder; the purity of the sample was checked by powder X-ray diffraction methods. The powder was loaded into a gelatine capsule. Magnetic measurements were carried out with a SQUID magnetometer (MPMS5, Quantum Design). The magnetic susceptibility measurements were made at 1000 G over the temperature range 5–300 K with a zero-field cooling (ZFC) procedure. Data were corrected for the diamagnetic contributions of the atomic cores [14].

2.4. Diffuse reflectance spectroscopy

An optical diffuse reflectance spectrum was measured at 293 K with a Cary 1E UV–Visible spectrophotometer equipped with a diffuse reflectance apparatus and a Varian Halon plate as a reference. Data were collected in the wavelength range 200–900 nm.

3. Results and discussion

$Pr_2Te_4O_{11}$ is isostructural with $Nd_2Te_4O_{11}$ [9], prepared in the same manner, and with $Ho_2Te_4O_{11}$ [10], prepared in an excess of TeO_2 as the flux. The structure of $Pr_2Te_4O_{11}$ viewed down the b-axis is displayed in Fig. 1. The PrO_8 polyhedron is a distorted square antiprism. The PrO_8 polyhedra share three O–O edges to form a network parallel to the (a,b) plane that can be formulated $^2_\infty[Pr_2O_{10}^{14-}]$ (Fig. 2). Within this bidimensional network, each PrO_8 polyhedron shares three edges with three similar

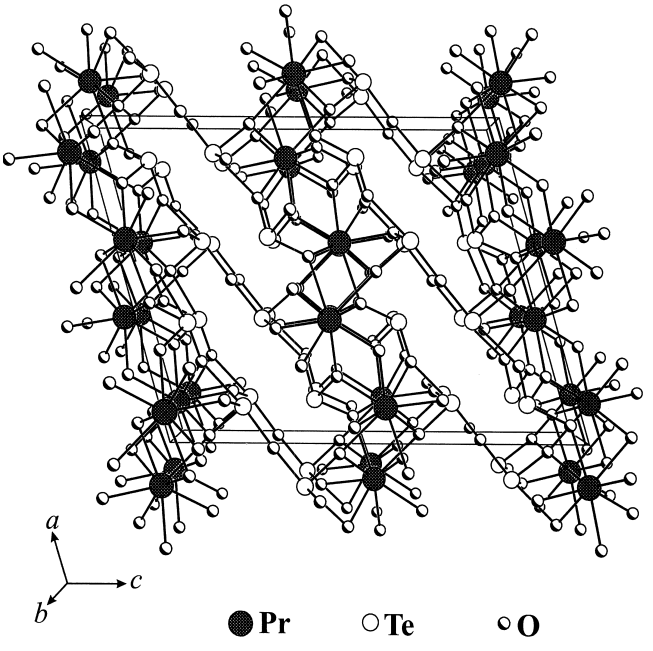

Fig. 1. View of the structure of $Pr_2Te_4O_{11}$ down the b-axis.

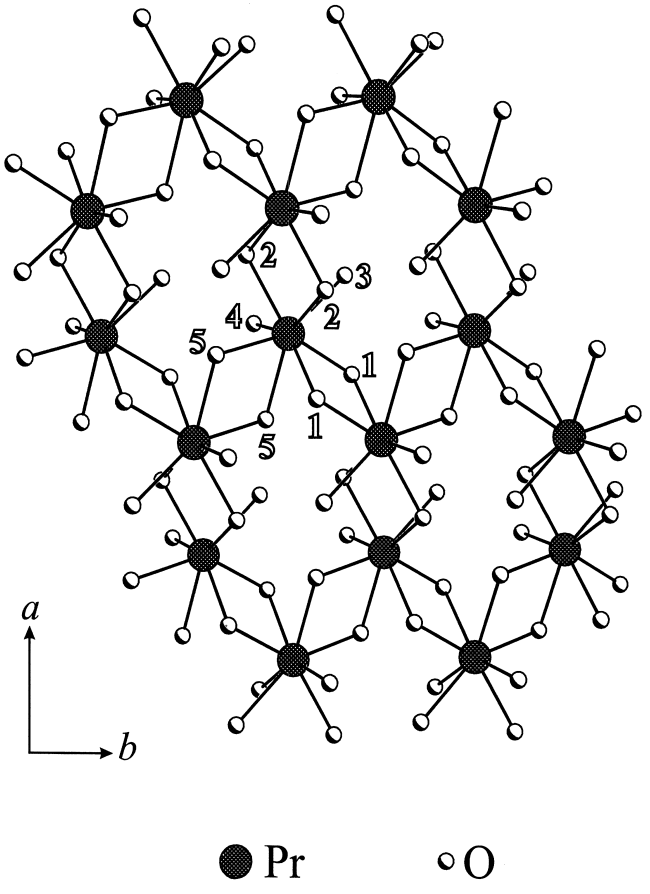

Fig. 2. View down [001] of the $^{2}_{\infty}[Pr_2O^{14-}_{10}]$ network in $Pr_2Te_4O_{11}$.

polyhedra. The Pr–O distances range from 2.375(2) to 2.615(2) Å (Table 3). These agree well with literature values, i.e. 2.418–2.628 Å in $PrPO_4$ [15] and 2.341–2.652 Å in $Pr_2W_2O_9$ [16].

Atom Te(1) is coordinated to three O atoms at distances of 1.834(2), 1.886(2), and 1.992(1) Å, with a longer distance at 2.451(2) Å; the analogous distances from atom Te(2) are 1.870(2), 1.883(2), 1.885(2), and 2.714(2) Å. As shown in Table 4, these Te–O distances are comparable to those found in $Nd_2Te_4O_{11}$ [9] and $Ho_2Te_4O_{11}$ [10] when the lanthanide contraction is taken into account. By sharing O corners, the TeO_4 polyhedra link to generate $^{2}_{\infty}[Te_4O^{6-}_{11}]$ layers parallel to the (*a*,*b*) plane (Fig. 3). These layers connect through corners to the $^{2}_{\infty}[Pr_2O^{14-}_{10}]$ network to form the three-dimensional structure.

Table 3
Selected interatomic distances (Å) and angles (°) for $Pr_2Te_4O_{11}$

	Pr–O(4)	2.375(2)	
	Pr–O(5)	2.385(2)	
	Pr–O(2)	2.401(2)	
	Pr–O(2)	2.425(2)	
	Pr–O(1)	2.505(2)	
	Pr–O(3)	2.509(2)	
	Pr–O(5)	2.574(2)	
	Pr–O(1)	2.615(2)	
Te(1)–O(4)	1.834(2)	Te(2)–O(5)	1.870(2)
Te(1)–O(1)	1.886(2)	Te(2)–O(2)	1.883(2)
Te(1)–O(6)	1.992(1)	Te(2)–O(3)	1.885(2)
Te(1)–O(3)	2.451(2)	Te(2)–O(1)	2.714(2)
O(4)–Te(1)–O(1)	103.36(8)	O(5)–Te(2)–O(2)	97.09(8)
O(4)–Te(1)–O(6)	91.36(9)	O(5)–Te(2)–O(3)	102.77(8)
O(1)–Te(1)–O(6)	95.75(6)	O(2)–Te(2)–O(3)	98.52(8)
O(4)–Te(1)–O(3)	89.17(7)	O(5)–Te(2)–O(1)	73.08(7)
O(1)–Te(1)–O(3)	77.63(7)	O(2)–Te(2)–O(1)	74.56(7)
O(6)–Te(1)–O(3)	173.29(5)	O(3)–Te(2)–O(1)	171.13(7)

To interpret the Te coordination, the bond valence model [17–19] can be applied. When only the three short Te–O interactions are considered, bond valences of 3.71 e^- for Te(1) and 3.91 e^- for Te(2) result. If the fourth distance is taken into account, then the bond valences are 3.99 e^- and 4.05 e^-, in good agreement with that expected for Te(IV) and with the values of 3.97 and 3.92 e^- calculated previously for $Nd_2Te_4O_{11}$ [9].

The magnetic susceptibility and the reciprocal susceptibility as a function of temperature for $Pr_2Te_4O_{11}$ are shown in Fig. 4. The compound shows Curie–Weiss paramagnetism over the temperature range 90–300 K, with $\chi = \chi_0 + C/(T - \theta_p)$ where $\chi_0 = 5.47.10^{-5}$ emu mol^{-1}, $C = 3.23(1)$ emu K^{-1} mol^{-1}, and $\theta_p = -15.2(2)$ K. The effective magnetic moment per Pr(III) cation obtained from the Curie constant C is 3.59(2) μ_B, in excellent agreement with the theoretical value of 3.58 μ_B [20]. The deviation from Curie–Weiss behavior at low temperature reflects the splitting of the ground state under the crystal field effect [20]. The negative value of the paramagnetic temperature θ_p is probably indicative of non-cooperative magnetic interactions [21–23]; to verify this would require a low-temperature neutron diffraction study.

The absorption spectrum of $Pr_2Te_4O_{11}$ (Fig. 5) shows a complex structure of sharp and well-resolved peaks between 420 and 520 nm. These bands originate from 4f–4f transitions of the $^3H_4$ ground state to the $^3P_0$, $^3P_1$, $^1I_6$, and $^3P_2$ excited states. The most intense transition is $^3P_2 \rightarrow {}^3H_4$. These transitions are responsible for the green color observed in Pr(III) compounds [24,25], whereas the $^1D_2 \rightarrow {}^3H_4$ transition around 600 nm has no influence on the color. In addition to these narrow spectral lines that arise from the f–f transitions of Pr(III), an optical absorption threshold at ~340 nm is observed. This corresponds to 3.65 eV, as deduced by means of a straightforward extrapolation method [26]. Comparable band gaps were recently found in the hydrothermally synthesized compounds $M_2Te_3O_8$ (M = Co: 3.60 eV; Ni: 3.84 eV; Cu: 2.64 eV) [27]. Wide band-gap semiconductors have attracted substantial interest for applications in solid-state electronics and optics [28–31].

Acknowledgements

This research was supported by the U.S. National Science Foundation under Grant DMR00-96676. Use was

Table 4
Comparisons among $Ln_2Te_4O_{11}$ compounds (Ln = Pr, Nd, Ho)

	$Pr_2Te_4O_{11}$	$Nd_2Te_4O_{11}$	$Ho_2Te_4O_{11}$
Reference	Present work	[9]	[10]
Preparation	CsCl flux, 1123 K	TeO_2 excess, 919 K	CsCl flux, 1073 K
Ln–O (Å)	2.375–2.615	2.385–2.603	2.259–2.514
Te(1)–O (Å)	1.834–1.992	1.830–1.989	1.834–2.010
	(2.451)	(2.434)	(2.357)
Te(2)–O (Å)	1.870–1.885	1.863–1.883	1.866–1.894
	(2.714)	(2.694)	(2.609)

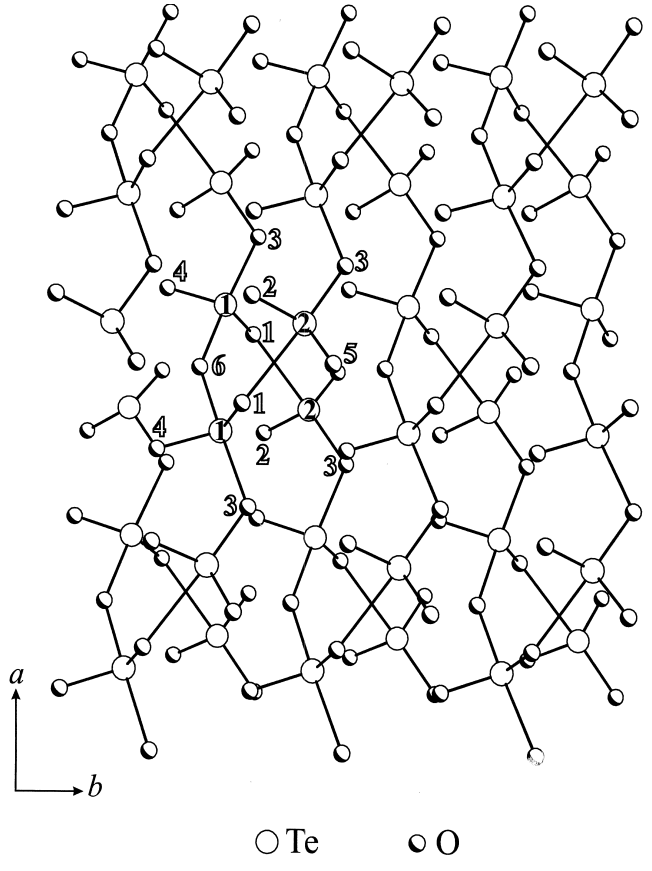

Fig. 3. $^{2}_{\infty}[Te_4O_{11}^{6-}]$ network in $Pr_2Te_4O_{11}$ as viewed down [001].

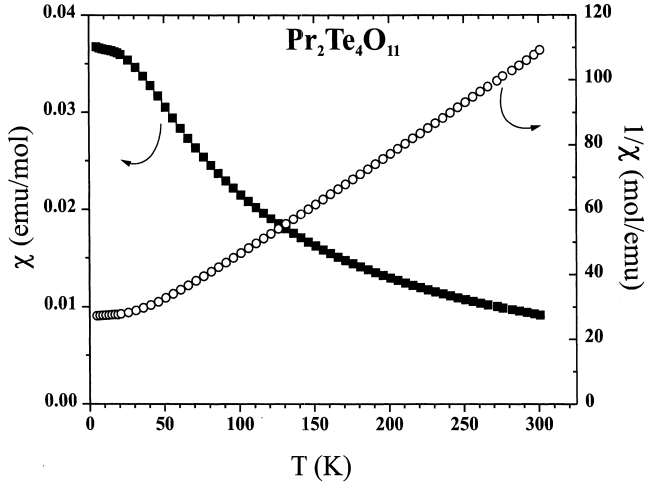

Fig. 4. χ and χ^{-1} versus T for $Pr_2Te_4O_{11}$. $H_{appl} = 1$ kG.

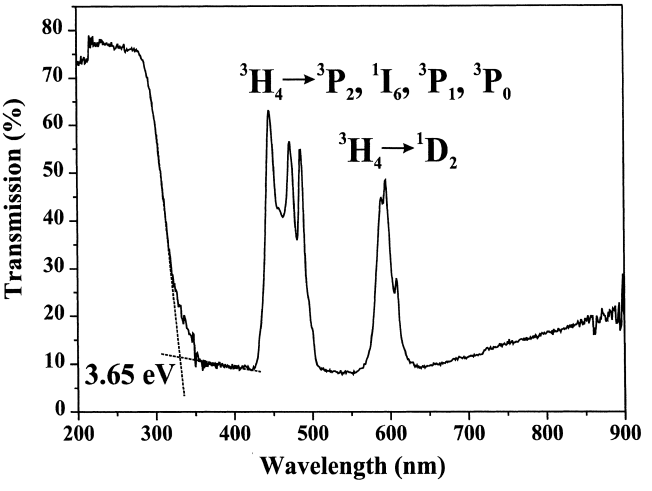

Fig. 5. Diffuse reflectance spectrum for $Pr_2Te_4O_{11}$.

made of the MRL Central Facilities supported by the National Science Foundation at the Materials Research Center of Northwestern University under Grant No. DMR00-76097.

References

[1] M.J. Redman, W.P. Binnie, J.R. Carter, J. Less-Common Met. 16 (1968) 407–413.
[2] C. Parada, J.A. Alonso, I. Rasines, Inorg. Chim. Acta 111 (1986) 197–199.
[3] M.L. López, M.L. Veiga, F. Fernández, A. Jerez, C. Pico, J. Less-Common Met. 166 (1990) 367–375.
[4] T. Endo, A. Shibuya, H. Takizawa, M. Shimada, J. Alloys Comp. 192 (1993) 50–52.
[5] C. Cascales, P. Porcher, R. Sáez-Puche, J. Phys. Chem. Solids 54 (1993) 1471–1474.
[6] C. Cascales, E. Antic-Fidancev, M. Lemaitre-Blaise, P. Porcher, J. Phys.: Condens. Matter 4 (1992) 2721–2734.
[7] G. Blass, Rev. Inorg. Chem. 5 (1983) 319–381.
[8] J. Galy, G. Meunier, S. Andersson, A. Åström, J. Solid State Chem. 13 (1975) 142–159.
[9] A. Castro, R. Enjalbert, D. Lloyd, I. Rasines, J. Galy, J. Solid State Chem. 85 (1990) 100–107.
[10] F.A. Weber, S.F. Meier, T. Schleid, Z. Anorg. Allg. Chem. 627 (2001) 2225–2231.
[11] Bruker SMART Version 5.054 Data Collection and SAINT-Plus Version 6.22 Data Processing Software for the SMART System, Bruker Analytical X-Ray Instruments, Inc., Madison, WI, USA, 2000.

[12] G.M. Sheldrick, SHELXTL DOS/Windows/NT Version 6.12, Bruker Analytical X-Ray Instruments, Inc., Madison, WI, USA, 2000.
[13] L.M. Gelato, E. Parthé, J. Appl. Crystallogr. 20 (1987) 139–143.
[14] L.N. Mulay, E.A. Boudreaux (Eds.), Theory and Applications of Molecular Diamagnetism, Wiley-Interscience, New York, 1976.
[15] D.F. Mullica, D.A. Grossie, L.A. Boatner, J. Solid State Chem. 58 (1985) 71–77.
[16] S.V. Borisov, R.F. Klevtsova, Kristallografiya 15 (1970) 38–42.
[17] I.D. Brown, Struct. Bonding Cryst. II (1981) 1–30.
[18] I.D. Brown, D. Altermatt, Acta Crystallogr. Sect. B Struct., Sci. 41 (1985) 244–247.
[19] N.E. Brese, M. O'Keeffe, Acta Crystallogr. Sect. B Struct., Sci. 47 (1991) 192–197.
[20] C. Kittel, Introduction to Solid State Physics, 6th Edition, Wiley, New York, 1986.
[21] A. Herpin, Théorie du Ferromagnétisme, Centre D'études Nucléaires de Saclay, Gif-sur-Yvette, France, 1957–1958.
[22] F. Brailsford, Physical Principles of Magnetism, Van Nostrand, London, 1966.
[23] C.J. O'Connor, Prog. Inorg. Chem. 29 (1982) 203–283.
[24] K. Binnemans, R. Van Deun, C. Görller-Walrand, J.L. Adam, J. Non-Cryst. Solids 238 (1998) 11–29.
[25] K. Binnemans, C. Görller-Walrand, Chem. Phys. Lett. 235 (1995) 163–174.
[26] O. Schevciw, W.B. White, Mater. Res. Bull. 18 (1983) 1059–1068.
[27] C.R. Feger, G.L. Schimek, J.W. Kolis, J. Solid State Chem. 143 (1999) 246–253.
[28] T. Taguchi, Y. Endoh, Jpn. J. Appl. Phys. 30 (1991) L952–L955.
[29] G. Sun, K. Shahzad, J.M. Gaines, J.B. Khurgin, Appl. Phys. Lett. 59 (1991) 310–311.
[30] M.A. Haase, J. Qiu, J.M. DePuydt, H. Cheng, Appl. Phys. Lett. 59 (1991) 1272–1274.
[31] C. Pong, N.M. Johnson, R.A. Street, J. Walker, R.S. Feigelson, R.C. De Mattei, Appl. Phys. Lett. 61 (1992) 3026–3028.